ACS OMEGA

http://pubs.acs.org/journal/acsodf

Article

Optimization of Gold Nanorod Features for the Enhanced Performance of Plasmonic Nanocavity Arrays

Marianna Beiderman,[§] Ariel Ashkenazy,[§] Elad Segal, Menachem Motiei, Adi Salomon, Tamar Sadan, Dror Fixler, and Rachela Popovtzer*

Cite This: *ACS Omega* 2021, 6, 29071−29077

Read Online

ACCESS | Metrics & More | Article Recommendations

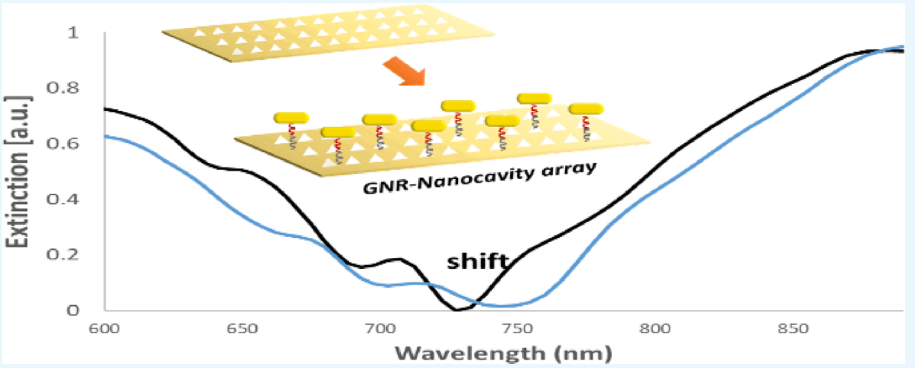

ABSTRACT: Nanoplasmonic biosensors incorporating noble metal nanocavity arrays are widely used for the detection of various biomarkers. Gold nanorods (GNRs) have unique properties that can enhance spectroscopic detection capabilities of such nanocavity-based biosensors. However, the contribution of the physical properties of multiple GNRs to resonance enhancement of gold nanocavity arrays requires further characterization and elucidation. In this work, we study how GNR aspect ratio (AR) and surface area (SA) modify the plasmonic resonance spectrum of a gold triangular nanocavity array by both simulations and experiments. The finite integration technique (FIT) simulated the extinction spectrum of the gold nanocavity array with 300 nm periodicity onto which the GNRs of different ARs and SAs are placed. Simulations showed that matching of the GNRs longitudinal peak, which is affected by AR, to the nanocavity array's spectrum minima can optimize signal suppression and shifting. Moreover, increasing SA of the matched GNRs increased the spectral variations of the array. Experiments confirmed that GNRs conjugated to a gold triangular nanocavity array of 300 nm periodicity caused spectrum suppression and redshift. Our findings demonstrate that tailoring of the GNR AR and SA parameters to nanoplasmonic arrays has the potential to greatly improve spectral variations for enhanced plasmonic biosensing.

INTRODUCTION

Nanoplasmonic biosensors are emerging as promising platforms for a wide range of medical and biological applications.[1−5] Nanoplasmonic biosensing is based on the surface plasmon resonance (SPR) in metallic thin films, generated through incident light that excites conduction band electrons in such metallic surfaces, giving rise to tightly confined optical fields.

Noble metal nanocavity arrays are particularly favorable for plasmonic biosensing because they exhibit extraordinary optical transmission (EOT) through subwavelength periodic arrays,[6,7] which enables simple readout, portability, and cost-effectiveness.[8] The binding of a target analyte to a plasmonic nanocavity array is sensed by spectral variation in the plasmonic resonance observed at either transmission maxima or transmission minima.[9] In particular, gold plasmonic nanocavity arrays of various types have distinct surface plasmon resonance (SPR) and are used for nanoplasmonic biosensing due to their biocompatibility and absorption spectrum in a visible range.[10,11]

Despite the advantages of plasmonic nanocavity arrays over conventional SPR schemes, such as portability and multiplexing capabilities, they generally have a lower bulk sensitivity.[12] The biosensing capabilities of such nanocavity arrays can be improved by enhancing the spectral variations in

Received: August 10, 2021
Accepted: September 22, 2021
Published: October 22, 2021

https://doi.org/10.1021/acsomega.1c04301
ACS Omega 2021, 6, 29071−29077

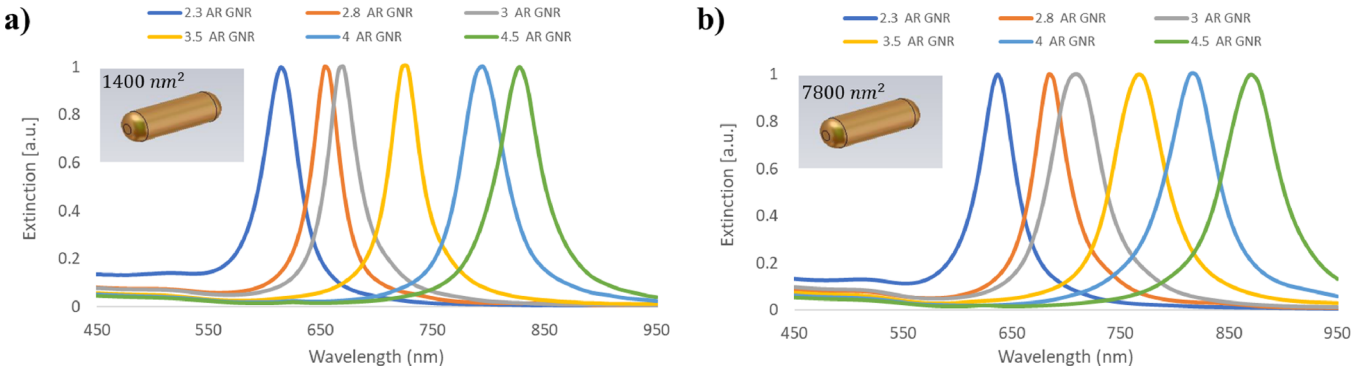

Figure 1. Simulation of LSPR spectra of GNRs of different ARs and SAs. (a) Extinction spectra of 1400 nm^2 GNRs at a range of ARs (2.3, 2.8, 3, 3.5, 4, and 4.5). (b) Extinction spectra of 7800 nm^2 GNRs at a range of ARs.

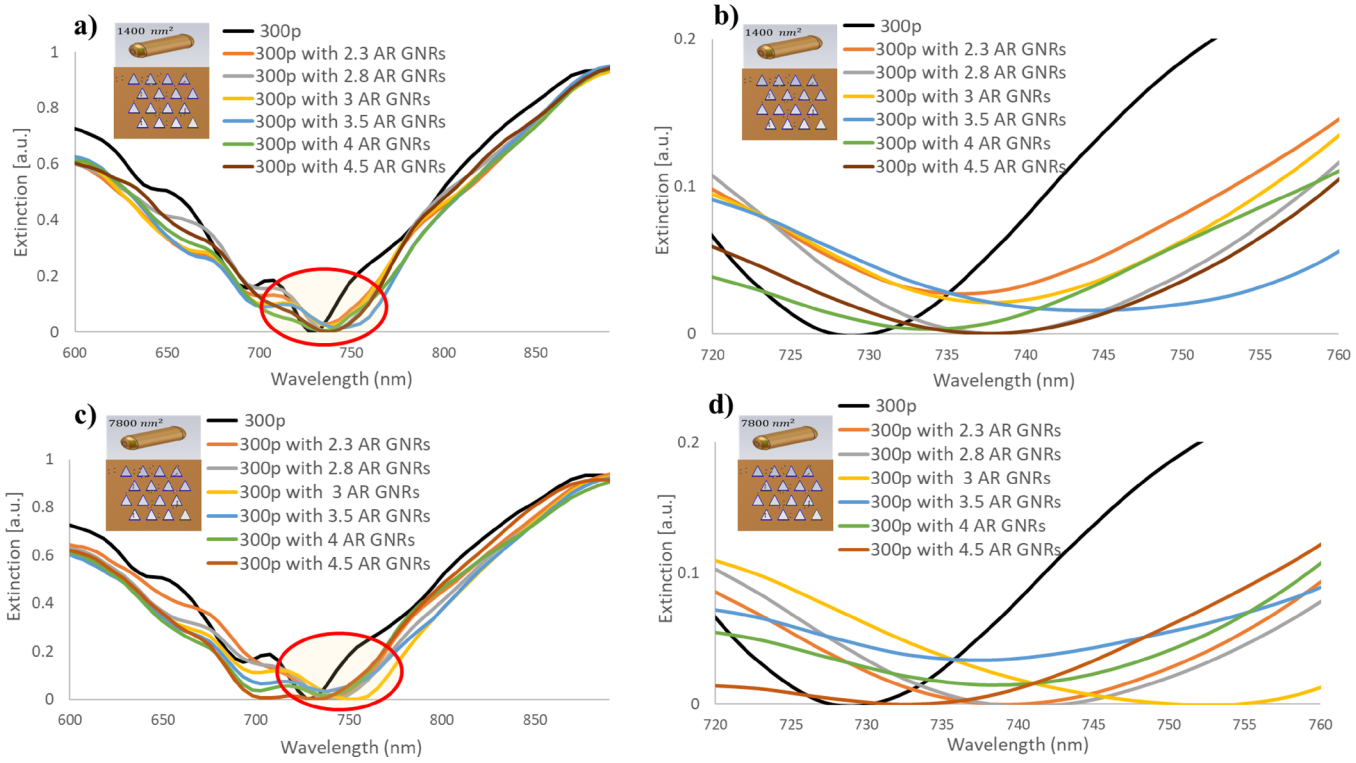

Figure 2. Simulation of a 300 p array with GNRs of different SAs and ARs. (a) Simulation of the spectra extinction of an isosceles triangular nanocavity array with or without 1400 nm^2 GNRs at a range of ARs (2.3−4.5). (b) Close-up of the minimal point (720−760 nm) of the simulated spectra (array with or without 1400 nm^2 GNRs). (c) Simulation of the spectra extinction of an isosceles triangular nanocavity array either with or without 7800 nm^2 GNRs at a range of ARs (2.3−4.5). (d) Close-up of the minimal point (720−760 nm) of the simulated spectra (array with or without 7800 nm^2 GNRs). GNRs were simulated at 18 nm proximity to the nanocavity array.

response to a target molecule binding.[13,14] To this end, efforts have focused on varying the thickness as well as the cavity size, structure, and periodicity of the nanocavity array, which affect their transmission spectrum and generate different plasmonic modes.[15−20] Another attractive approach for enhancing the spectral variation of nanocavity arrays is by incorporating gold nanorods (GNRs), which have unique optical properties[21−24] that enhance spectroscopic processes.[8,10,25,26] We previously demonstrated that GNRs conjugated to a gold nanocavity array enable biomarker detection for biosensing applications.[11]

GNRs are straightforward to synthesize and enable simple control over their size and aspect ratio (AR).[10,27,28] GNRs have two plasmonic modes: the transverse mode at ∼520 nm and the longitudinal plasmon mode in the near-infrared (NIR) region. These modes make GNRs favorable for utilization within biological tissues requiring penetration depth. Unlike the transverse plasmon mode, the GNR's longitudinal plasmon mode is affected by the AR and is redshifted with increased AR.[29]

To further improve the performance of nanocavity array biosensing platforms, there is need to elucidate the effect of GNRs' physical properties on such platforms and find optimal parameters for the increase of the array's spectral variations.[30] Herein, we investigated the AR and SA parameters of GNRs to be utilized together with a nanocavity array for spectral shift enhancement. Using an electromagnetic field simulation software, we simulated a gold triangular nanocavity array with GNRs of different AR and surface area (SA) combinations. The finite integration technique (FIT),[31] a powerful method for computing the optical scattering of

https://doi.org/10.1021/acsomega.1c04301
ACS Omega 2021, 6, 29071−29077

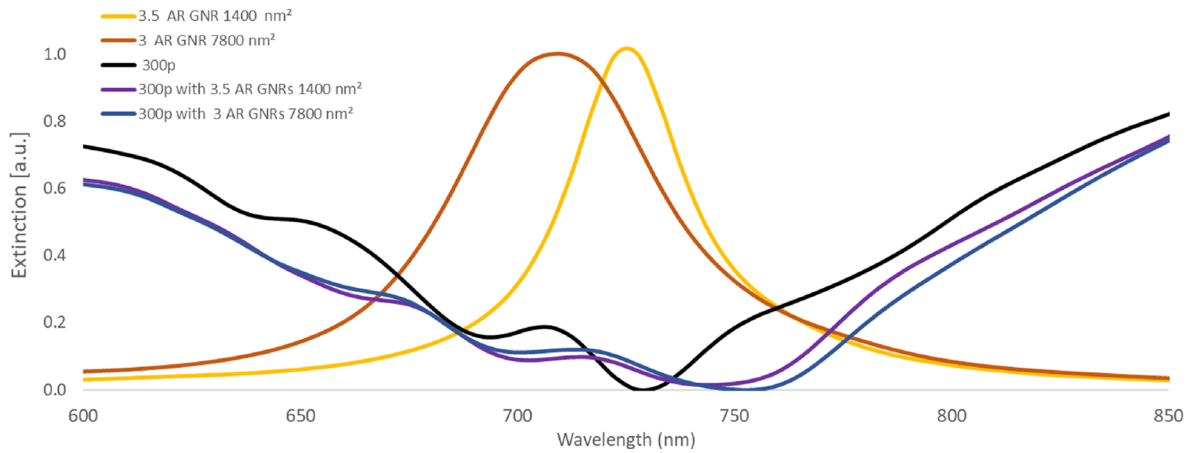

Figure 3. Simulation of the extinction of the highest spectra-shifting GNRs. Shown are the simulated spectra of 1400 nm^2 GNR having 3.5 AR, 7800 nm^2 GNR having 3 AR, the 300 p nanocavity array alone, and the 300 p nanocavity array together with GNR (1400 nm^2 GNR with 3.5 AR and 7800 nm^2 GNR with 3 AR).

nonspherical particles,[32] was used to calculate the theoretical extinction spectra of GNRs onto a plasmonic nanocavity array. An experimental study confirmed the transmission spectrum variation of a GNR-conjugated gold nanocavity array. We found that the GNR's AR and SA enable spectral variation enhancement by selecting GNRs with larger SA and by matching of the GNRs' longitudinal peak with the nanocavity array transmission minima. The results demonstrate that FIT enables the selection of optimal GNR AR and SA parameters to be utilized together with the nanocavity array for spectral shift enhancement.

RESULTS

We first simulated GNRs of different SAs (1400 and 7800 nm^2) and at a range of ARs (2.3, 2.8, 3, 3.5, 4, and 4.5) using an electromagnetic field simulation software and applied FIT calculations to determine their maximum longitudinal localized SPR (LSPR) spectra (Figure 1a,b). Our results for both GNR sizes showed that with the increase in AR, the absorption longitudinal peak shows more redshift. This is in agreement with experimental results of other studies.[29,33] Furthermore, comparison between the two SAs (Figure 1a,b) shows an effect on both the shift and width of the longitudinal peak; i.e., an increase in the SA of GNRs, with the same AR, enhanced the longitudinal resonance peak and broadened the resonance. This is likely due to an extra damping effect.[32,34] It is noteworthy that 1400 nm^2 GNRs with an AR of 3.5 and 7800 nm^2 GNRs with an AR of 3 had closer longitudinal peaks than smaller and larger GNRs with the same AR. This indicates that not only the AR but also the size of GNRs affects the GNR's transmission spectrum.[32,34] We also note that there was a smaller transverse mode peak in the simulation spectra at ∼530 nm as compared to the absorption spectra observed in experimental measurements that were reported in the literature.[10,29] This difference between simulation and experiments spectra has been discussed in the literature, for example, by Link et al., who justified this by the fact that the absorption band in the experimental spectrum is a superposition of the transverse mode of the GNRs and a result of spherical gold particle impurities created during GNR synthesis.[29,35] This causes the transversal mode to be more pronounced in experiments than in simulations.

Next, we studied the effect of GNRs with different SA and AR combinations on the spectral shift of a nanocavity array. Based on our previously reported biosensor nanocavity array,[11,16] which incorporated triangular nanocavities as part of a bio-barcode sensor for enzymatic detection, we simulated a nanocavity array (Figure 2) composed of isosceles triangular nanocavities (≈200 nm long base and ≈215 nm long sides), with 300 nm periodicity (300 p) between nanocavities. GNRs were simulated with either smaller (1400 nm^2) or larger (7800 nm^2) SA, and a range of ARs as above (2.3−4.5), each at 18 nm proximity to the nanocavity array. GNRs were randomly oriented above the array and excitation was linearly polarized, with 45° polarization relative to the nanotriangles' height (Methods).

FIT simulations demonstrated that the different GNRs suppressed and shifted the nanocavity array's resonance spectrum from the 727 nm minima point of the nanocavity array alone (Figure 2). For smaller GNRs (1400 nm^2), the largest shift in nanocavity array spectrum minima was observed for an AR of 3.5, showing a 15.8 nm shift as compared to nanocavity array alone (from 727.7 to 743.5 nm; Figure 2a,b). For larger GNRs (7800 nm^2), the highest shift in nanocavity array spectrum was observed for GNRs with an AR of 3, showing a shift of 26.8 nm as compared to nanocavity array alone (from 727.7 to 754.4 nm; Figure 2c,d). Larger GNRs with an AR of 3 showed a larger shift in the array's resonance spectrum (11 nm more) as compared to the shift caused by smaller GNRs with an AR of 3.5.

Taken together, these results indicate stronger variations in resonance with increased SA of GNRs.

Next, we focused on the two GNRs above that produced the largest spectral shift in the nanocavity array: 1400 nm^2 GNRs with an AR of 3.5 and 7800 nm^2 GNRs with an AR of 3. The longitudinal peak of these simulated GNRs alone closely matched the resonance spectrum minima point of the nanocavity array alone. Moreover, simulation of either GNR type upon the nanocavity array showed that the larger GNR produced a greater suppression in the spectra of the nanocavity array and a stronger redshift at the transmission minima point of the nanocavity array (Figure 3). Thus, by matching the GNRs' longitudinal plasmonic peak, which is affected by both AR and size, to the nanocavity array minima, we obtained the largest resonance variation in the array's spectrum.

https://doi.org/10.1021/acsomega.1c04301
ACS Omega 2021, 6, 29071−29077

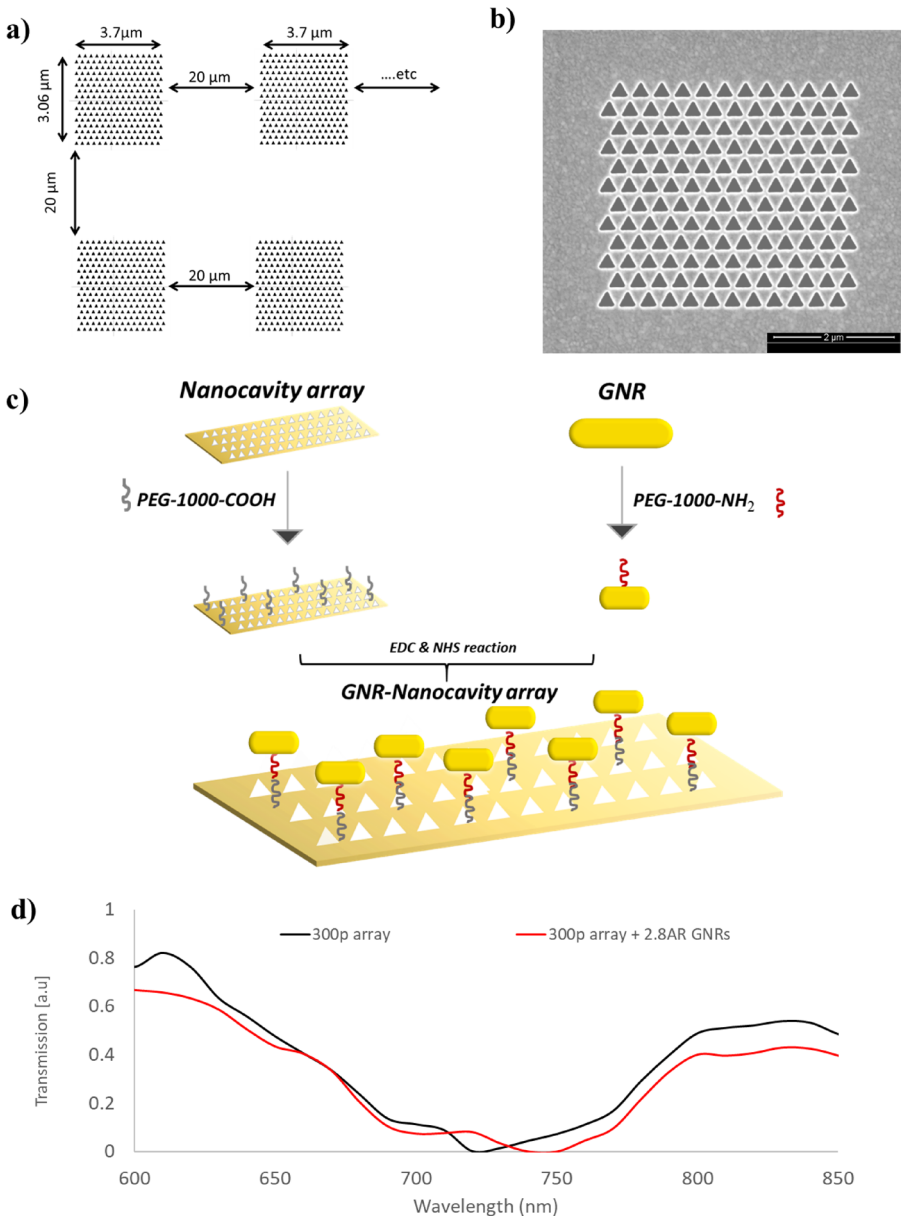

Figure 4. Experiment with 300 p nanocavity array and GNRs. (a) Scheme of the sensing array. Four representative regions are shown out of the 10 × 10 regions of 12 × 12 triangular nanocavities. The size of each region (3.7 × 3.06 μm) and the distances between each region (20 μm) are indicated. (b) Image of the nanocavity array acquired by HSEM. (c) Scheme of the experimental system. GNRs were conjugated to a gold nanocavity array at an approximate distance of 18 nm (for each GNR). (d) Transmission spectrum of the 300 p array alone and 300 p array with 2.8 AR GNRs (71 nm length, 25 nm diameter).

To validate the simulation results, we conducted experiments with GNRs and a nanocavity array. Based on our previous study with a GNR-conjugated nanocavity array,[11] we fabricated a 300 p nanocavity array consisting of a gold film (100 nm; Platypus Technologies) milled with isosceles triangular nanocavities by a focused ion beam.[16] The array was fabricated to have 10 × 10 nanocavity regions, with 20 μm distance between each region, and a total size of 217 × 210 μm. Each region (3.7 × 3.06 μm) consisted of 12 × 12 triangular nanocavities of ≈200 nm long base and ≈220 nm long sides[16] with 300 nm periodicity between each cavity (Figure 4a). A high scanning electron microscope (HSEM) confirmed the dimensions and structure of the nanocavity array (Figure 4b). The nanoarray was then coated with a PEG linker, and GNRs with an AR of 2.8 (25 × 71 nm; longitudinal peak at 650 nm; Nanopartz Inc.) were conjugated to the array's surface (Methods) at a distance of ∼18 nm from the array (Figure 4c). SPR transmission measurements of the nanocavity array alone showed an absorption peak at 610 nm with an additional peak at 820 nm (minimum point at 720 nm), and the GNR-conjugated array showed a 10 nm shift of the minimum point (Figure 4d). This finding is very similar to the simulation results, confirming the effect of GNRs on spectral variations of a nanocavity array.

DISCUSSION

In the present study, we explored the effect of GNRs with different sizes and ARs on the transmission spectrum variation of a gold nanocavity array. Our results indicate that both AR and SA of GNRs affect the plasmonic interaction with the

https://doi.org/10.1021/acsomega.1c04301
ACS Omega 2021, 6, 29071−29077

nanocavity array surface. We found that by changing GNRs' AR, the longitudinal plasmon resonance peak can be altered to match the nanocavity array transmission minima for the enhancement of resonance variations. Further, we found that with an increase in GNR size, larger spectral variations are observed. The size of GNRs affects the plasmonic nanocavity array resonance by suppressing its transmission spectrum and causing a redshift. These phenomena are caused by the coupling of the GNRs' plasmonic modes to those of the nanocavity array, which locally distorts its near-field, producing suppression and shifting of the transmission spectrum in the far field.

Previous studies have shown plasmonic mode enhancement of the nanocavity array by tuning the structure and distance between nanocavities.[15,16] Here, our findings demonstrate that tuning the nanocavity array's plasmonic mode to match the GNR's LSPR resonance peak can also result in additional plasmonic mode enhancement by the increase of spectral variations. Belushkin et.al conducted seminal work in the field of nanoplasmonic biosensors and developed a portable and digital plasmonic imager consisting of a gold nanoparticle-enhanced nanocavity array. This imager enabled the rapid detection of biomarkers and provided equivalent performance to that of gold-standard laboratory assays.[8,19] Our findings with a triangular nanocavity array, in combination with GNRs, have potential for further detection optimization of plasmonic biosensors. The unique combination of GNRs and a gold isosceles triangular nanocavity array is expected to enable the improvement of detection by the increase in spectral variations and opens new opportunities for NIR imaging for *in vivo* applications.

Our findings also demonstrate that FIT simulation can serve as a guidance for choosing specific GNR physical parameters for the best performance and system enhancement of a nanocavity array. FIT simulations could also be used in the future to choose a specific nanocavity array periodicity together with GNR parameters for enhancing system performance. Tuning the periodicity of nanocavity arrays allows multiplex sensing of various factors, such as hormones, antibodies, antigens, enzymes, and nucleotides.[26,36] Thus, future work will investigate the effect of different nanocavity array features, such as periodicity, together with GNRs with differing physical features, on spectral variations. This has a potential to further enhance the abilities of nanoplasmonic biosensors. Incorporating florescence in the nanocavity array can add an additional dimension for multiplexed sensing and produce metal-enhanced fluorescence[37] to be used for *in vivo* applications.

In conclusion, our findings indicate that by tailoring the physical parameters of GNRs to a nanocavity array, we can enhance the plasmonic resonance distortion of the array by signal suppression and shifting. A larger surface area of GNRs, as well as correlation of the GNR's longitudinal mode with the spectrum minima point of a nanocavity array, has the potential to increase spectral variations for improved detection that is especially important when small quantities of analyte are present. Thus, the proposed approach can be applied to optimizing plasmonic sensing of nanocavity arrays for various point-of-care applications.

METHODS

Plasmonic Nanocavity Array Synthesis and Characterization. A 100 nm gold film (on top of a 22 mm glass slide; Platypus Technologies) was milled by a focused ion beam (Helios NanoLab Dual Beam 600, FEI) to yield 10 × 10 nanocavity regions. Each region (3.7 × 3.06 μm) consisted of 12 × 12 triangular nanocavities of ≈200 nm long base and ≈220 nm long sides with 300 nm periodicity between each cavity. There was a 20 μm distance between each region, and the total size of the regions was 217 × 210 μm. Characterization was done by HSEM (Helios NanoLab Dual Beam 600) and SPR measurements (described below). The gold film was then coated with SH-poly(ethylene glycol) (PEG)−COOH (Sigma-Aldrich) by leaving to stir in purified water for 3 h. The size of PEG (1 kDa) was selected to ensure a distance of ∼10 nm from the gold film surface to the GNRs for interaction between the nanocavity array and GNRs.

GNR Coating, Characterization, and Conjugation to the Gold Film. Bare GNRs in CTAB (GNR650) sized 25 × 71 nm, with an aspect ratio of 2.8 (Nanopartz Inc., USA.), were centrifuged for 5 min under 3500*g* to remove CTAB excess; coated with PEG-Amine from Creative PegWorks (HS-PEG-NH_2, MW 1k); and left stirring for 3 h.[38] The coated GNRs were centrifuged three times for 10 min under 4500*g* to remove the PEG-Amine excess. To confirm the coating, GNR absorption spectra were measured using a UV-1650PC (Shimadzu Corporation, Kyoto, Japan) and ζ charge measurements (ZetaSizer 3000HS; Malvern Instruments, Malvern, UK).[39,40] We found that following the coating of GNRs, the peak of the absorption spectra shifted by 5 nm, and the charge of the GNRs increased due to PEG-1000-amine coating. These results confirm the successful coating of the GNRs.

To ensure a sufficient quantity of GNRs for conjugation to the gold nanocavity array, the GNR concentration was calculated using flame atomic emission spectrometry.

To cross-link between the GNRs and the gold nanocavity array, 1-ethyl-3-(3-dimethylaminopropyl)-carbodiimide (EDC) and *N*-hydroxysuccinimide (NHS) (Sigma-Aldrich) were added to conjugate GNRs and the gold nanocavity array and were left stirring together for 3 h.

SPR Measurements. A Nikon Eclipse 80i microscope was used to take SPR measurements. The nanocavity array was illuminated in a bright field mode by nonpolarized light. Magnification of ×40 (NA = 0.95) objective was used to take the spectra, and transmission spectra were recorded by a spectrophotometer connected to a charge coupled device camera (CCD). The Nuance software was used to subtract the background in the measurements.

Simulations. Simulations were performed using CST Studio Suite 2021 (Dassault Systèmes, France), a Maxwell's equation solver based on the finite integration technique.[31] We used the time-domain solver, with −100 dB accuracy for the simulations of GNRs and −50 dB for the simulations of the triangular nanocavity array. For all simulations, a hexahedral mesh type was used (30 cells per wavelength), with open boundaries. To extract the extinction spectra of the simulated models, a broadband far-field monitor was defined, with 121 samples and 10^{-3} accuracy.

The dielectric function of gold was taken from the famous report by Johnson and Christy.[41] Simulations of the extinction spectrum of GNR with a length of 75 nm and a diameter of 25 nm were conducted for a range of values for the dielectric constant of the environment, and the results were compared to the known experimental extinction spectrum of such GNR. A dielectric constant of ε_r = 1.45 for the environment yielded results that were most similar to the experimental spectrum; thus, we have chosen this value for the simulations.

https://doi.org/10.1021/acsomega.1c04301
ACS Omega 2021, 6, 29071−29077

GNRs of various sizes were simulated, all with the shape of a hemispherically capped cylinder. For the simulations of triangular nanocavities arrays, we simulated an array of 100 nm thickness with 4 × 4 triangular nanocavities. The triangles were isosceles with a base length of 200 nm and side lengths of 215 nm. The distance between centers of neighboring triangles was 300 nm. Twenty-two randomly oriented GNRs were placed 18 nm above the array in a plane parallel to it. This configuration was kept the same throughout all array simulations with GNRs and the nanocavity array.

The models were excited by a plane wave at normal incidence. The excitation was linearly polarized, with 45° polarization relative to the GNRs' long axis (in GNR simulations) or nanotriangles' height (in array simulations).

AUTHOR INFORMATION

Corresponding Author

Rachela Popovtzer − *Faculty of Engineering and the Institute of Nanotechnology and Advanced Materials, Bar Ilan University, Ramat Gan 5290002, Israel*; Email: rachela.popovtzer@biu.ac.il

Authors

Marianna Beiderman − *Faculty of Engineering and the Institute of Nanotechnology and Advanced Materials, Bar Ilan University, Ramat Gan 5290002, Israel*; orcid.org/0000-0003-0110-121X

Ariel Ashkenazy − *Faculty of Engineering and the Institute of Nanotechnology and Advanced Materials, Bar Ilan University, Ramat Gan 5290002, Israel*

Elad Segal − *Department of Chemistry, Institute of Nanotechnology and Advanced Materials, Bar Ilan University, Ramat Gan 5290002, Israel*; orcid.org/0000-0002-6354-0907

Menachem Motiei − *Faculty of Engineering and the Institute of Nanotechnology and Advanced Materials, Bar Ilan University, Ramat Gan 5290002, Israel*

Adi Salomon − *Department of Chemistry, Institute of Nanotechnology and Advanced Materials, Bar Ilan University, Ramat Gan 5290002, Israel*; orcid.org/0000-0002-5643-0478

Tamar Sadan − *Faculty of Engineering and the Institute of Nanotechnology and Advanced Materials, Bar Ilan University, Ramat Gan 5290002, Israel*; orcid.org/0000-0002-8305-3778

Dror Fixler − *Faculty of Engineering and the Institute of Nanotechnology and Advanced Materials, Bar Ilan University, Ramat Gan 5290002, Israel*; orcid.org/0000-0003-0963-7908

Complete contact information is available at: https://pubs.acs.org/10.1021/acsomega.1c04301

Author Contributions

§M.B. and A.A. contributed equally to this work.

Notes

The authors declare no competing financial interest.

ACKNOWLEDGMENTS

This work was partially supported by the Israel Ministry of Science and Technology grant number 3-16491 and grant number 3-14345. The work of M.B. in this study was supported by the Israel Ministry of Science and Technology Golda Meir Academy-Industry grant for Advancement of Woman in Science.

REFERENCES

(1) Jackman, J. A.; Linardy, E.; Yoo, D.; Seo, J.; Ng, W. B.; Klemme, D. J.; Wittenberg, N. J.; Oh, S. H.; Cho, N. J. Plasmonic Nanohole Sensor for Capturing Single Virus-Like Particles toward Virucidal Drug Evaluation. *Small* **2016**, *12*, 1159−1166.

(2) Masson, J. F. Surface Plasmon Resonance Clinical Biosensors for Medical Diagnostics. *ACS Sensors* **2017**, *2*, 16−30.

(3) Bocková, M.; Slabý, J.; Špringer, T.; Homola, J. Advances in Surface Plasmon Resonance Imaging and Microscopy and Their Biological Applications. *Annu. Rev. Anal. Chem.* **2019**, *12*, 151−176.

(4) Lopez, G. A.; Estevez, M. C.; Soler, M.; Lechuga, L. M. Recent Advances in Nanoplasmonic Biosensors: Applications and Lab-on-a-Chip Integration. *NANO* **2017**, *6*, 123−136.

(5) Ankri, R.; Meiri, A.; Lau, S. I.; Motiei, M.; Popovtzer, R.; Fixler, D. Intercoupling Surface Plasmon Resonance and Diffusion Reflection Measurements for Real-Time Cancer Detection. *J. Biophotonics* **2013**, *6*, 188−196.

(6) Ghaemi, H. F.; Thio, T. Extraordinary Optical Transmission through Sub-Wavelength Hole Arrays. *ature* **1998**, *391*, 667−669.

(7) Lezec, H. J.; Pellerin, K. M.; Thio, T.; Pendry, J. B.; Ebbesen, T. W. Theory of Extraordinary Optical Transmission through Sub-wavelength Hole Arrays. *Phys. Rev. Lett.* **2001**, *86*, 1114.

(8) Belushkin, A.; Yesilkoy, F.; Altug, H. Nanoparticle-Enhanced Plasmonic Biosensor for Digital Biomarker Detection in a Microarray. *ACS Nano* **2018**, *12*, 4453−4461.

(9) Jackman, J. A.; Rahim Ferhan, A.; Cho, N. J. Nanoplasmonic Sensors for Biointerfacial Science. *Chem. Soc. Rev.* **2017**, *46*, 3615−3660.

(10) Eustis, S.; El-Sayed, M. A. Why Gold Nanoparticles Are More Precious than Pretty Gold: Noble Metal Surface Plasmon Resonance and Its Enhancement of the Radiative and Nonradiative Properties of Nanocrystals of Different Shapes. *Chem. Soc. Rev.* **2006**, *35*, 209−217.

(11) Beiderman, M.; Ashkenazy, A.; Segal, E.; Barnoy, E. A.; Motiei, M.; Sadan, T.; Salomon, A.; Rahimipour, S.; Fixler, D.; Popovtzer, R. Gold Nanorod-Based Bio-Barcode Sensor Array for Enzymatic Detection in Biomedical Applications. *ACS Appl. Nano Mater.* **2020**, *3*, 8414−8423.

(12) Sener, G.; Ozgur, E.; Rad, A. Y.; Uzun, L.; Say, R.; Denizli, A. Rapid Real-Time Detection of Procalcitonin Using a Microcontact Imprinted Surface Plasmon Resonance Biosensor. *Analyst* **2013**, *138*, 6422−6428.

(13) Oh, S. H.; Altug, H. Performance Metrics and Enabling Technologies for Nanoplasmonic Biosensors. *Nat. Commun.* **2018**, *9*, 5263.

(14) Li, X., Soler, M., Szydzik, C., Khoshmanesh, K., Schmidt, J., Yesilkoy, F., Belushkin, A., Coukos, G., Mitchell, A., Altug, H., *"An Integrated Nanoplasmonic Biosensor for Monitoring Cytokine Secretion from Single Cells,"* In: 2019 15th Conference on Ph. D Research in Microelectronics and Electronics (PRIME). IEEE, 2019. p. 113-116.

(15) Segal, E.; Weissman, A.; Gachet, D.; Salomon, A. Hybridization between Nanocavities for a Polarimetric Color Sorter at the Sub-Micron Scale. *Nanoscale* **2016**, *8*, 15296−15302.

(16) Weissman, A.; Galanty, M.; Gachet, D.; Segal, E.; Shavit, O.; Salomon, A. Spatial Confinement of Light onto a Flat Metallic Surface Using Hybridization between Two Cavities. *Adv. Opt. Mater.* **2017**, *5*, 1700097.

(17) Fischer, L. M.; Tenje, M.; Heiskanen, A. R.; Masuda, N.; Castillo, J.; Bentien, A.; Émneus, J.; Jakobsen, M. H.; Boisen, A. Gold Cleaning Methods for Electrochemical Detection Applications. *Microelectron. Eng.* **2009**, *86*, 1282−1285.

(18) Lindquist, N. C.; Lesuffleur, A.; Im, H.; Oh, S. Sub-Micron Resolution Surface Plasmon Resonance Imaging Enabled by Nano-hole Arrays with Surrounding Bragg Mirrors for Enhanced Sensitivity and Isolation. *Lab Chip* **2009**, *9*, 382−387.

(19) Belushkin, A.; Yesilkoy, F.; González-López, J. J.; Ruiz-Rodríguez, J. C.; Ferrer, R.; Fàbrega, A.; Altug, H. Rapid and Digital

Detection of Inflammatory Biomarkers Enabled by a Novel Portable Nanoplasmonic Imager. *Small* **2020**, *16*, 1906108.
(20) Barnoy, E. A.; Fixler, D.; Popovtzer, R.; Nayhoz, T.; Ray, K. An Ultra-Sensitive Dual-Mode Imaging System Using Metal-Enhanced Fluorescence in Solid Phantoms. *Nano Res.* **2015**, *8*, 3912−3921.
(21) Ankri, R.; Melzer, S.; Tarnok, A.; Fixler, D. Detection of Gold Nanorods Uptake by Macrophages Using Scattering Analyses Combined with Diffusion Reflection Measurements as a Potential Tool for in Vivo Atherosclerosis Tracking. *Int. J. Nanomed.* , *10*, 4437−4446, DOI: 10.2147/IJN.S86615.
(22) Ankri, R.; Fixler, D. Gold Nanorods Based Diffusion Reflection Measurements: Current Status and Perspectives for Clinical Applications. *NANO* **2017**, 1031−1042.
(23) Betzer, O.; Ankri, R.; Motiei, M.; Popovtzer, R. Theranostic Approach for Cancer Treatment: Multifunctional Gold Nanorods for Optical Imaging and Photothermal Therapy. *J. Nanomater.* **2015**, *2015*, 1.
(24) Liu, X.; Liu, L.; Hu, X.; Zhou, S.; Ankri, R.; Fixler, D.; Xie, Z. Multimodal Bioimaging Based on Gold Nanorod and Carbon Dot Nanohybrids as a Novel Tool for Atherosclerosis Detection. *Nano Res.* **2018**, *11*, 1262−1273.
(25) Mauriz Elba, D. P.; L, L. M. Advances in Nanoplasmonic Biosensors for Clinical Applications. *Analyst* **2019**, *144*, 7105−7129.
(26) Soler, M.; Belushkin, A.; Cavallini, A.; Kebbi-Beghdadi, C.; Greub, G.; Altug, H. Multiplexed Nanoplasmonic Biosensor for One-Step Simultaneous Detection of Chlamydia Trachomatis and Neisseria Gonorrhoeae in Urine. *Biosens. Bioelectron.* **2017**, *94*, 560−567.
(27) Elliott, E. N.; Kaestner, K. H. *HHS Public Access* **2016**, *72*, 4139−4156.
(28) Burrows, N. D.; Lin, W.; Hinman, J. G.; Dennison, J. M.; Vartanian, A. M.; Abadeer, N. S.; Grzincic, E. M.; Jacob, L. M.; Li, J.; Murphy, C. J. Surface Chemistry of Gold Nanorods. *Langmuir* **2016**, *32*, 9905−9921.
(29) Link, S.; Mohamed, M. B.; El-Sayed, M. A. Simulation of the Optical Absorption Spectra of Gold Nanorods as a Function of Their Aspect Ratio and the Effect of the Medium Dielectric Constant. *J. Phys. Chem. B* **1999**, *103*, 3073−3077.
(30) Li, G. C.; Zhang, Q.; Maier, S. A.; Lei, D. Plasmonic Particle-on-Film Nanocavities: A Versatile Platform for Plasmon-Enhanced Spectroscopy and Photochemistry. *NANO* **2018**, *7*, 1865−1889.
(31) Clemens, M.; Weiland, T. Discrete Electromagnetism with the Finite Integration Technique. *Prog. Electromagn. Res.* **2001**, *32*, 65−87.
(32) Lee, K. S.; El-Sayed, M. A. Dependence of the Enhanced Optical Scattering Efficiency Relative to That of Absorption for Gold Metal Nanorods on Aspect Ratio, Size, End-Cap Shape, and Medium Refractive Index. *J. Phys. Chem. B* **2005**, *109*, 20331−20338.
(33) Jorge, P.; Pastoriza-santos, I.; Liz-marz, L. M.; Mulvaney, P. Gold Nanorods : Synthesis , Characterization and Applications. *Coord. Chem. Rev.* **2005**, *249*, 1870−1901.
(34) Khlebtsov, B. N.; Khlebtsov, N. G. Multipole Plasmons in Metal Nanorods: Scaling Properties and Dependence on Particle Size, Shape, Orientation, and Dielectric Environment. *J. Phys. Chem. C* **2007**, *111*, 11516−11527.
(35) Link, S., Ratio, A., ″) (1) 2 2,″ 109(20), 10531−10532 (2005).
(36) Coskun, A. F.; Cetin, A. E.; Galarreta, B. C.; Alvarez, D. A.; Altug, H.; Ozcan, A. Lensfree Optofluidic Plasmonic Sensor for Real-Time and Label-Free Monitoring of Molecular Binding Events over a Wide Field-of-View. *Sci. Rep.* **2015**, *4*, 1−7.
(37) Ji, B.; Deorukhkar, A. Targeting Pancreatic Cancer with Magneto-Fluorescent Theranostic Gold Nanoshells. *Nanomedicine* **2014**, *9*, 1209−1222.
(38) Jakobsohn, K.; Motiei, M.; Sinvani, M.; Popovtzer, R. Towards Real-Time Detection of Tumor Margins Using Photothermal Imaging of Immune-Targeted Gold Nanoparticles. *Int. J. Nanomed.* **2012**, *7*, 4707−4713.
(39) Zhou, Y.; Hu, Y.; Sun, W.; Lu, S.; Cai, C.; Peng, C.; Yu, J.; Popovtzer, R.; Shen, M.; Shi, X. Radiotherapy-Sensitized Tumor Photothermal Ablation Using γ-Polyglutamic Acid Nanogels Loaded with Polypyrrole. *Biomacromolecules* **2018**, *19*, 2034−2042.
(40) Shwartz, A.; Betzer, O.; Kronfeld, N.; Kazimirsky, G.; Cazacu, S.; Finniss, S.; Lee, H. K.; Motiei, M.; Dagan, S. Y.; Popovtzer, R.; et al. Therapeutic Effect of Astroglia-like Mesenchymal Stem Cells Expressing Glutamate Transporter in a Genetic Rat Model of Depression. *Theranostics* **2017**, *7*, 2690−2703.
(41) Johnson, P. B.; Christy, R. W. Optical Constant of the Nobel Metals. *Phys. L Re View B* **1972**, *6*, 4370−4379.

https://doi.org/10.1021/acsomega.1c04301
ACS Omega 2021, 6, 29071−29077